Journal of Materials Chemistry C

PAPER

View Article Online
View Journal | View Issue



Cite this: J. Mater. Chem. C, 2014, 2, 5357

# Effect of crystallinity in small molecular weight organic heterojunction solar cells†

Hiroyuki Saeki,[ab] Omi Kurimoto,[a] Haruka Nakaoka,[b] Masahiro Misaki,[a] Daiki Kuzuhara,[b] Hiroko Yamada,*[bc] Kenji Ishida*[a] and Yasukiyo Ueda[a]

Received 27th January 2014
Accepted 13th April 2014

DOI: 10.1039/c4tc00183d

www.rsc.org/MaterialsC

Planar-heterojunction (PHJ; pn) solar cells were fabricated using a thermally convertible well soluble benzoporphycene (BPc) precursor and [6,6]-phenyl-$C_{61}$-butyric acid methyl ester ($PC_{61}BM$). The conversion temperature was controlled in order to investigate the influence of the crystallinity of the organic semiconducting layer in the PHJ solar cell on the cell performance. The crystallinity of BPc increased with annealing temperature, but the surface roughness did not change. The cell with BPc converted at 250 °C had a power conversion efficiency that was 2.5 times better (1.49%) than that of the cell converted at 150 °C, and 1.5 times better than the cell with a vacuum-deposited BPc layer. The mobility of BPc, measured from the space charge limited current characteristics, supports a clear correlation between crystallinity and cell performance. Thus, the importance of increasing the crystallinity and mobility in organic solar cells was experimentally demonstrated.

## Introduction

Organic photovoltaic (OPV) cells have attracted significant interest as a promising route to low-cost, lightweight and flexible energy sources.[1] Recent advances in OPV cells have provided 10% power conversion efficiency (PCE), which places them in direct competition with PV cells based on amorphous silicon.[2] The improvement in PCE has been strongly accelerated by modification of the molecular structure to match the sunlight spectrum and by control of the phase-separated structure in the donor–acceptor mixed thin film.[3] The crystallinity and mobility of the materials are key factors to improve the OPV cell performance.[4] However, a clear correlation between the crystallinity and cell performance has not yet been determined.

The crystallization of organic semiconductors in bulk-heterojunction (BHJ) cells progresses with heat treatment or solvent annealing.[5] In these crystallization processes, the area of the donor–acceptor interface also changes, which makes it impossible to accurately estimate. Thus, it is difficult to analyze the correlation between the crystallinity and cell performance. Conjugated polymers are not suitable for the fabrication of pn planar-heterojunction (PHJ) cells due to their solubility in common solvents used for fabrication of the upper layer. However, PHJ cells can be fabricated by the evaporation of small semiconducting molecules. The small molecules exhibit higher crystallinity than the conjugated polymers. The crystallinity, surface roughness, and molecular orientation of the film are strongly dependent on the substrate temperature during the vacuum-deposition process.

Macrocyclic π-conjugated molecules, such as phthalocyanines and porphyrins, have been widely investigated as photoactive materials for OPV cells. These molecules are generally processed using vacuum deposition to obtain thin films, due to their low solubility in organic solvents. Over the past decade, precursors of benzoporphyrin (BP) with four bicycle [2.2.2]octadiene (BCOD) structures at the β-positions of the pyrroles have been developed for the solution processing of BP.[6] The precursors are converted into BP by annealing at 200 °C with the elimination of four ethylene molecules. The converted BP thin film becomes an insoluble polycrystalline film. This process makes it possible to realize pn or pin structures by spin-coating without dissolution of the lower layer. A pin junction OPV cell with the BP precursor has exhibited a high PCE of 5.2%.[7] This precursor method is not only for the fundamental study of OPV cells, but for practical application. Although there have been several reports on soluble precursors such as anthracene,[8] pentacene,[9] oligothiophene,[10] quinacridone[11] and phthalocyanine,[12] even these molecules have room for improvement in their absorption characteristics. Thus, one important challenge is to develop semiconducting molecules that possess a wide absorption band in the visible to near-IR (NIR) region for the improvement of the OPV cell performance.

[a]Graduate School of Materials Science, Nara Institute of Science and Technology, 8916-5, Ikoma, Nara 630-0192, Japan. E-mail: hyamada@ms.naist.jp; Fax: +81-743-72-6042; Tel: +81-743-72-6041

[b]Graduate School of Science and Technology, Kobe University, Kobe, 657-8501, Japan

[c]CREST, JST, Chiyoda-ku, 102-0075, Japan

† Electronic supplementary information (ESI) available: Experimental conditions, synthesis route, NMR, crystal structure data, TG, IR and SCLC data. See DOI: 10.1039/c4tc00183d

Benzoporphycene (BPc) is a constitutional isomer of BP with two direct bonds and two ethenyl bridges between neighboring isoindoles.[13] Compared with BP, BPc has a low-symmetry molecular structure and displays broad absorption bands in the visible region. To use BPc in a wet process, we have previously prepared a thermally-convertible BPc precursor (BPc-pre-1) with BCOD substituents, as shown in Fig. 1, and evaluated the film formation and conversion behavior of BPc-pre-1.[14] However, BPc-pre-1 was poorly soluble in organic solvents, with a solubility of 0.15% (w/w) in dichloromethane. The thickness of a BPc-pre-1 film fabricated by spin-coating was only 20 nm, which was insufficient for application as the photoactive layer of an OPV cell.

In this paper, a dimethyl-BCOD fused BPc precursor (BPc-pre-2) (shown in Fig. 1) was synthesized to realize sufficient solubility for wet processing. The more bulky substituents enable BPc-pre-2 to be readily dissolved in solvents,[15] due to a reduction of intermolecular aggregation in the film. OPV cells with BPc converted from BPc-pre-2 as a p-type semiconductor and [6,6]-phenyl-$C_{61}$-butyric acid methyl ester (PCBM) as an n-type semiconductor were fabricated and compared with OPV cells of BPc prepared from BPc-pre-1 and PCBM. The PHJ structure was selected because it is first reported in the BPc-pre-2. Though the BHJ cell provides a large pn interface and high performance, the conversion to BPc and phase separation progress at the same time. This situation makes difficult to accurately discuss the potential of the BPc converted from BPc-pre-2. Here, we conduct a fundamental study of OPV cells to determine the correlation between crystallinity and cell performance, by preparing PHJ cells that utilize highly crystalline and insoluble BPc films.

## Results and discussion

BPc-pre-2 was prepared from ethyl 4,7-dihydro-8,8′-dimethyl-4,7-ethano-2*H*-isoindole-1-carboxylate[15] using the same synthesis procedure as that for BPc-pre-1 (ESI, Scheme S1, Fig. S1–6†).[13a] The structure of a BPc-pre-2 crystal grown in a mixture of 2-propanol and chlorobenzene was confirmed by single crystal X-ray diffraction analysis (ESI, Fig. S7†). The single crystal contains two chlorobenzenes per BPc-pre-2 molecule in a unit cell. To improve the purity of BPc-pre-2, we examined further purification with gel permeation chromatography (GPC) using chloroform as an eluent and recrystallization from chloroform/methanol. The recrystallized BPc-pre-2 was dried overnight under vacuum to remove adsorbed chloroform and methanol. The $^1$H nuclear magnetic resonance (NMR) spectrum of BPc-pre-2 in deuterated dichloromethane showed several methyl singlet peaks at 1.45–1.51 and 0.54–0.65 ppm (ESI, Fig. S6†), which indicated that BPc-pre-2 consists of structural isomers, as was the case for the previously reported dimethyl BCOD-fused porphyrin.[15] Chloroform protons were observed at 7.32 ppm with an abundance ratio of 1 : 0.75 for BPc-pre-2 : chloroform. On the other hand, no methanol signals were observed. Thus, the BPc-pre-2 crystal included chloroform as a crystal solvent, which is analogous with the chlorobenzene included in the single crystal. Thermogravimetric (TG) analysis was conducted to investigate the thermal conversion behavior of BPc-pre-2. When dried BPc-pre-2 powder was annealed (ESI, Fig. S8†), the weight loss was observed over the temperature range from 125 to 210 °C, as was the case for BPc-pre-1.[13a] The total weight loss was 37.0%, which was consistent with the loss of four isobutene molecules and a chloroform molecule. It was also confirmed that dried BPc-pre-2 powder included chloroform, which was used in the recrystallization process.

The color of the BPc-pre-2 thin film changed from blue to green with annealing. Fig. 2 shows the UV-vis absorption spectra of BPc-pre-2 films on an indium tin oxide (ITO)/poly(3,4-ethylenedioxythiophene) : poly(styrene sulfonate) (PEDOT : PSS) substrate before and after annealing at 200 °C for 10 min. The absorption spectrum of the as-spun BPc-pre-2 film exhibited a Soret band at around 390 nm and a Q-band between 550 and 700 nm. After annealing, the Soret band was red-shifted to 450 nm, and the Q-band extended to 750 nm. The shape of the spectrum of the BPc film produced from BPc-pre-2 also corresponded to that produced from BPc-pre-1.[14a] There were no differences between the precursors except for the absorbance, which derives from the film thickness. The thicknesses for BPc-pre-2 and BPc-pre-1 were 80 and 20 nm, respectively. Fig. 2 also shows a spectrum for a vacuum-deposited BPc film, which is consistent with that for the film converted from BPc-pre-2. A Fourier transform-infrared (FT-IR) spectrum of the BPc-pre-2 film

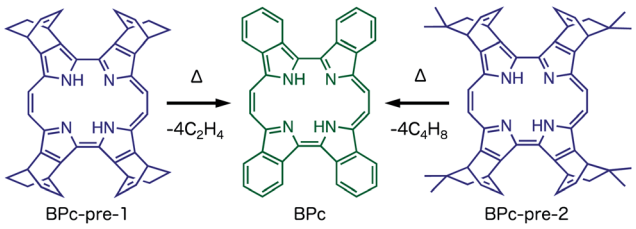


Fig. 1 Reaction scheme for the formation of BPc from BPc-pre-1 and 2.

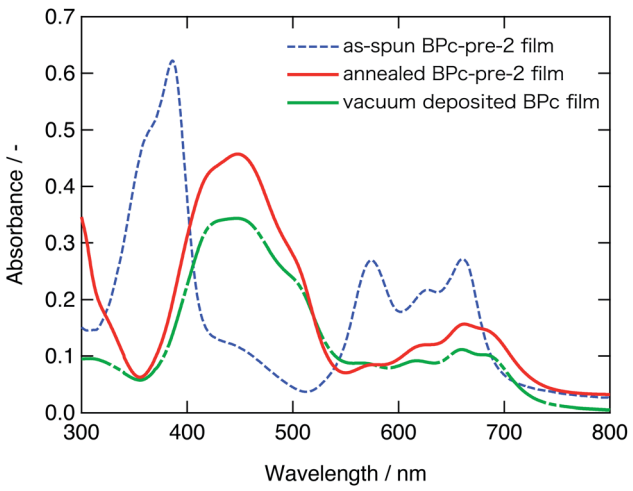


Fig. 2 UV-vis absorption spectra of a vacuum-deposited BPc film, and a BPc-pre-2 film before and after annealing at 200 °C for 10 min.

after annealing for 10 min revealed the disappearance of the $\nu$(C–H) vibration modes for the methylene (2865, 2937, and 2954 $cm^{-1}$) and methyl (1382 and 1450 $cm^{-1}$) groups, and the appearance of absorption bands at 734, 812, 888, 1446 and 1602 $cm^{-1}$ (ESI, Fig. S9†). Therefore, it was concluded that the retro-Diels–Alder reaction was terminated by annealing under this condition, which was also confirmed by the end of the weight loss in the TG profile. The conversion time was dependent on the annealing temperature, as shown in Table. 1, where increasing the annealing temperature increased the conversion rate to BPc, which was determined by the disappearance of absorption bands for BPc-pre-2 from the UV-vis and FT-IR spectra. The annealing time for device fabrication was set to approximately twice the conversion time, which would ensure that all BPc-pre-2 was converted to BPc in the film.

The as-spun BPc-pre-2 film was smooth, with a root-mean-square (RMS) roughness of about 0.2 nm (Fig. 3(a)). The high resolution electron diffraction (HRED) pattern of the as-spun film showed a halo pattern (Fig. 3(b)), which indicates that the BPc-pre-2 film was amorphous. Fig. 3(c) shows an atomic force microscopy (AFM) image of the BPc-pre-2 film after annealing at 200 °C for 10 min (*i.e.*, BPc film). Although there were many small pores that seem to be generated by the desorption of leaving groups, the surface roughness was significantly improved compared to the BPc-pre-1 film.[14a] The selected area electron diffraction (SAED) pattern obtained from a circular area with a diameter of 1 μm showed a ring pattern projected along the $b$*-axis of the BPc crystal (triclinic, $a$ = 5.536 Å, $b$ = 14.502 Å, $c$ = 14.754 Å, $\alpha$ = 98.633°, $\beta$ = 91.079°, and $\gamma$ = 96.534°) (Fig. 3(d)).[13a] This indicates that the (010) planes in the BPc crystal are parallel to the substrate surface and BPc molecules take an edge-on orientation, which is the same as that observed for the BPc film converted from BPc-pre-1.[14a] Fig. 3(e) and (f) show an AFM image and SAED pattern for the vacuum-deposited BPc film, respectively. The surface of the vacuum-deposited BPc film was rougher than the BPc film converted from BPc-pre-2, but also had the same edge-on molecular orientation. During the vacuum-deposition process, molecules migrate extensively on the substrate surface and crystallize, which results in the formation of grains and a roughened surface. In the case of BPc-pre-1, the precursor aggregates and then converts into BPc, which produces a discontinuous BPc film.[14a] The bulky substituents of BPc-pre-2 reduces the amount of intermolecular aggregation in the film, so that BPc-pre-2 is converted to BPc before aggregation and the BPc subsequently crystallizes, which results in a smooth and continuous BPc film.

Fig. 4 shows current–voltage ($J$–$V$) curves for OPV cells with BPc film converted from BPc-pre-2 and with a vacuum-deposited BPc film. The photovoltaic parameters for the OPV cells

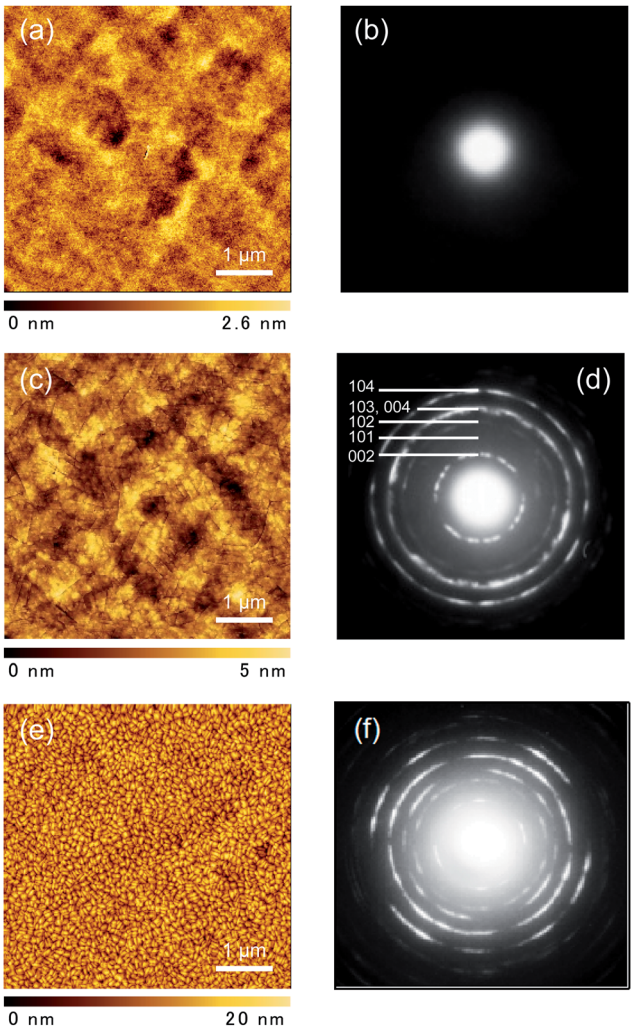


Fig. 3 (a and b) AFM images and HRED patterns of the as-spun BPc-pre-2 film. AFM image and SAED pattern for (c and d) the BPc-pre-2 film after annealing at 200 °C for 10 min, and (e and f) vacuum-deposited BPc film.

Table 1 Conversion time and annealing time for device fabrication at several temperatures

| Temp. °C | 150 | 170 | 200 | 250 |
|---|---|---|---|---|
| Conversion time | 120 | 48 | 8 | 1.5 |
| Annealing time | 240 | 120 | 20 | 3 (min) |

fabricated from vacuum-deposited BPc, BPc-pre-1[14b] and BPc-pre-2 films, such as the short circuit current density ($J_{SC}$), open circuit voltage ($V_{OC}$), fill factor (FF), and power conversion efficiency (PCE) are summarized in Table 2.

The performance of the OPV cell with the film prepared from BPc-pre-2 was significantly better than the reported performance for cells using BPc-pre-1,[14b] which indicates improvement of the p-layer thin film continuity and the formation of good PHJs in the cell. The performance of the OPV cells strongly depends on the annealing temperature. When annealed at 150 °C, a PCE of 0.61% was obtained. An increase in the annealing temperature to 170 and 200 °C increased the PCE to 1.19 and 1.29%, respectively. Further improvement of the device performance was achieved at 250 °C, with $V_{OC}$ = 0.47, $J_{SC}$ = 5.35, FF = 0.59, and the resulting PCE was 1.49%. The PCE of OPV cells with BPc-pre-2 film annealed at over 170 °C surpassed the performance of even the vacuum-deposited BPc film.

Fig. 5 shows an incident photon to current conversion efficiency (IPCE) spectrum for an OPV cell fabricated with BPc-per-2

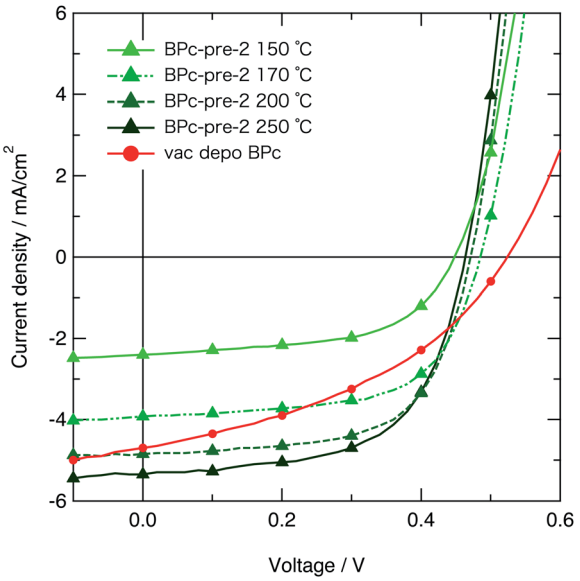


Fig. 4 *J–V* curves for OPV cells with BPc film converted from BPc-pre-2 and with vacuum-deposited BPc film.

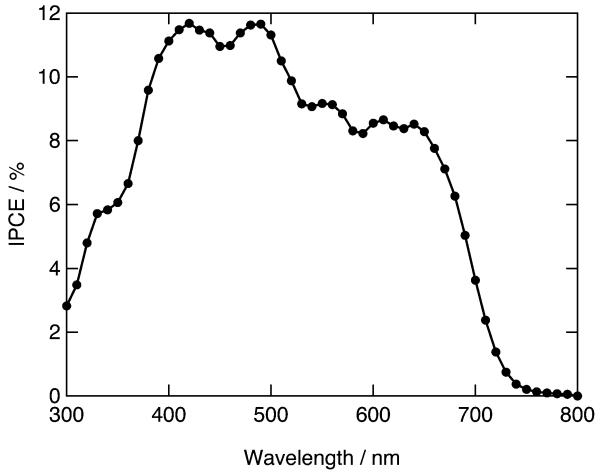


Fig. 5 IPCE spectrum for an OPV cell prepared from the BPc-pre-2 film annealed at 250 °C.

film annealed at 250 °C. The IPCE is defined as the number of photogenerated charge carriers that contribute to the photocurrent per incident photon. The cell showed a broad spectral response from 400 to 700 nm, which is derived from the continuity of the Soret band and Q-band of BPc. Thus, the low symmetry of the molecular structure was effective for broad absorption in the visible region.[7]

To analyze the enhancement of $J_{SC}$ with increased annealing temperature, the detailed morphology of the BPc film was investigated using AFM, transmission electron microscopy (TEM) and X-ray diffraction (XRD) measurements. After annealing at 150 °C, some aggregates were observed in the AFM image (Fig. 6(a)); however, the height of grains was less than 5 nm and the number of grains was small, so that it could be considered a flat surface. In addition, no diffraction spots were observed in the SAED pattern (Fig. 6(b)). When annealing at 170 °C (Fig. 6(c)) and 200 °C (Fig. 3(c) former shown), a small domain with an area of *ca.* 100 nm was clearly observed from the height contrast. The diffraction spots also became clear and spot-like (Fig. 6(d) and Fig. 3(d)). When annealed at 250 °C, a unique morphology with many small aligned cracks was observed (Fig. 6(e)). SAED indicated a single net pattern projected along the *b**-axis of the BPc crystal (Fig. 6(f)). Fig. 6(g) shows a superposition of the TEM image and the SAED pattern for the BPc film prepared at 250 °C. The angle between the crack directions (dotted lines) and the *a**-axis was ±37°; the cracks were parallel to the (207) and (20–7) planes of the BPc crystals. Therefore, the (207) and (20–7) planes in the lattice are parallel to the herringbone packed molecular plane of BPc (Fig. 6(h)). BPc crystals are thus easily cleaved at the molecular planes to relax the strain associated with crystallization, which results in the formation of a herringbone surface texture. Though the crystallinity was changed by the annealing temperature, the ratio of area, calculated by (the surface area calculated from the roughness)/(sweeping area by AFM), was almost constant in each film. Therefore, the increase of $J_{SC}$ is not due to the increase of the interface.

Fig. 7 shows XRD patterns of BPc films prepared at several temperatures from 150 to 250 °C. The BPc films showed only diffraction peaks at 6.1° and 12.2°, which correspond to (010) and (020) reflections. This is consistent with the SAED patterns shown in Fig. 3(d) and 6(a)–(c). The peak intensity increased with annealing temperature. The crystallite size was also estimated by using the full width at half maximum (FWHM) of the diffraction peaks and Scherrer equation. Each crystallite size of the converted BPc film was as follows, 15.9 nm (150 °C), 24.6 nm (170 °C), 28.0 nm (200 °C) and 24.2 nm (250 °C), respectively. To briefly summarize the film structure, the BPc films prepared from BPc-pre-2 had sufficiently smooth surfaces to be used in

Table 2 Photovoltaic parameters for OPV cells and calculated hole mobilities for BPc films produced at several temperatures

| Material | Temp. (°C) | $J_{SC}$ [mA cm$^{-2}$] | $V_{OC}$ [V] | FF [–] | PCE [%] | Mobility [cm$^2$ V$^{-1}$ s$^{-1}$] |
|---|---|---|---|---|---|---|
| BPc-pre-1 | 200 | 0.36 | 0.02 | 0.25 | $1.8 \times 10^{-3}$ | |
| BPc-pre-2 | 150 | 2.40 | 0.45 | 0.57 | 0.61 | $1.69 \times 10^{-5}$ |
| | 170 | 3.95 | 0.48 | 0.63 | 1.19 | $1.14 \times 10^{-4}$ |
| | 200 | 4.85 | 0.47 | 0.61 | 1.40 | $3.83 \times 10^{-4}$ |
| | 250 | 5.35 | 0.47 | 0.59 | 1.49 | $1.01 \times 10^{-3}$ |
| Vac. depo. BPc | | 4.70 | 0.52 | 0.40 | 0.99 | |

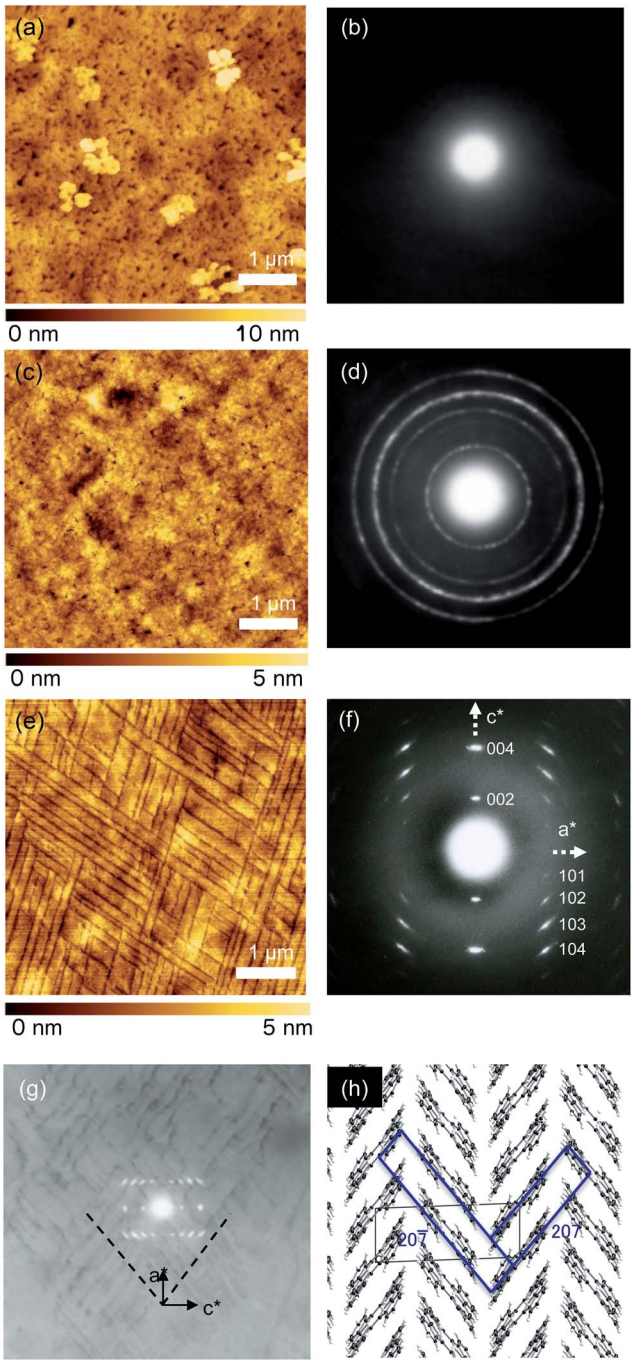


Fig. 6 AFM images and SAED patterns of the BPc film produced at (a and b) 150 °C, (c and d) 170 °C, and (e and f) 250 °C. The SAED patterns were obtained from a circular area with a diameter of 1 μm. (g) Superposition of a TEM image and SAED pattern of the BPc film prepared at 250 °C. The dotted lines show the direction of cracks. (h) Schematic image of the molecular packing in a BPc film.

PHJ cells. The BPc films consistently assumed the same edge-on orientation. The decrease in the amorphous regions enables the carriers to pass effectively, which results in an increase in $J_{SC}$.

$J_{SC}$ is the sum of $J_{SC,h}$ and $J_{SC,e}$ (eqn (1)). We can assume that $J_{SC,e}$ is negligibly small in the BPc film; therefore, $J_{SC}$ through

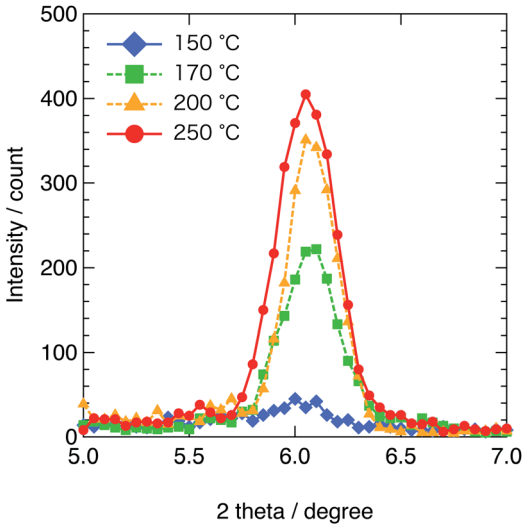


Fig. 7 XRD patterns of BPc films prepared at temperatures from 150 to 250 °C.

the BPc film can be expressed using the linear sum of the drift hole current and the diffusion hole current, as given by eqn (2):

$$J_{SC} = J_{SC,h} + J_{SC,e}, \quad (1)$$

$$J_{SC} = q\left(p\mu_h E - D_h \frac{dp}{dx}\right), \quad (2)$$

where $q$ is the elementary charge, $p$ is the concentration of holes, $E$ is the internal electrical field, and $D_h$ is the hole diffusion constant. The variable constants are $p$ and the hole mobility ($\mu_h$). $p$ was compared by enhancing the carrier with negative high bias (−2 V) on OPV cells[16] utilizing BPc films (ESI, Fig. S10†). In this regime, all of the charges can effectively be swept out regardless of the mobilities. The current of all the devices converged to about 7 mA cm.$^{-2}$ This result enables to treat $p$ as a constant. Therefore, $J_{SC}$ is primarily determined by $\mu_h$. For BPc thin films, $\mu_h$ has been investigated using space charge limited current (SCLC) measurements with hole-only devices.[17] Fig. 8 shows the dark current for ITO/PEDOT:PSS/BPc/Au devices corrected by the $V$–$V_{bi}$.[18] $V_{bi}$ is the built in potential extracted from the $I$–$V$ curve. The SCLC behavior can be described by:

$$J = \frac{9}{8}\mu\varepsilon_0\varepsilon'\frac{V^2}{L^3}, \quad (3)$$

where $\varepsilon_0$ is the vacuum permittivity, $\varepsilon'$ is the relative dielectric constant of the organic films, $\mu$ is the charge carrier mobility, and $L$ is the thickness of the organic film.[19] The relative dielectric constant was assumed to be 3.0. The mobility was calculated from the current in the square law region, and is also summarized in Table 2.

The film prepared at 150 °C had the lowest mobility of $1.69 \times 10^{-5}$ cm$^2$ V$^{-1}$ s$^{-1}$. For the BPc films, $\mu_h$ increased with annealing temperature and reached $1.01 \times 10^{-3}$ cm$^2$ V$^{-1}$ s$^{-1}$ for the film prepared at 250 °C, which is approximately 60 times of that for the film prepared at 150 °C. The change in mobility with

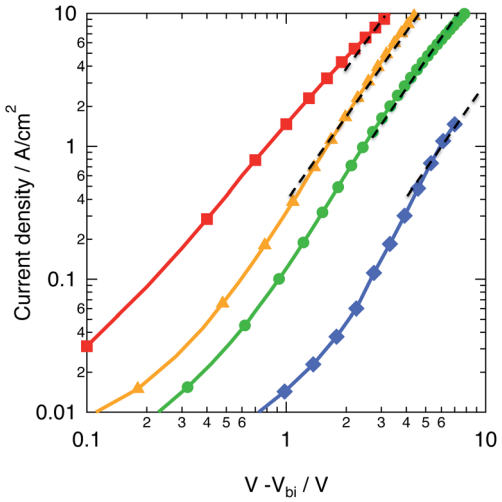


Fig. 8 *J–V* characteristics of ITO/PEDOT:PSS/BPc/Au devices.

annealing temperature was due to the increase in crystallinity, as supported by the XRD analysis. High crystallinity leads to an enhancement of both the mobility and $J_{SC}$, resulting in enhancement of PCE.

Fig. 9 shows the dependence of $J_{SC}$ and FF on hole mobility. $J_{SC}$ was saturated, despite the increase in the hole mobility in the BPc film. Enhancement of the mobility has recently been reported to increase the FF;[20] however, the FF did not increase in OPV cells with crystallized BPc. This can be explained by the effect of PCBM on the electron mobility ($\mu_e$). The $\mu_e$ value for PCBM was determined to be $1.03 \times 10^{-4}$ cm$^2$ V$^{-1}$ s$^{-1}$ from SCLC measurements using an electron-only device (ESI, Fig. S11†). This is comparable to the mobility of the BPc films fabricated at 150 or 170 °C. The imbalance between the hole and electron mobility in OPV cells fabricated at 200 and 250 °C gave rise to a $J_{SC}$ plateau and a constant FF. The development of highly crystalline electron transport layers will open the door to

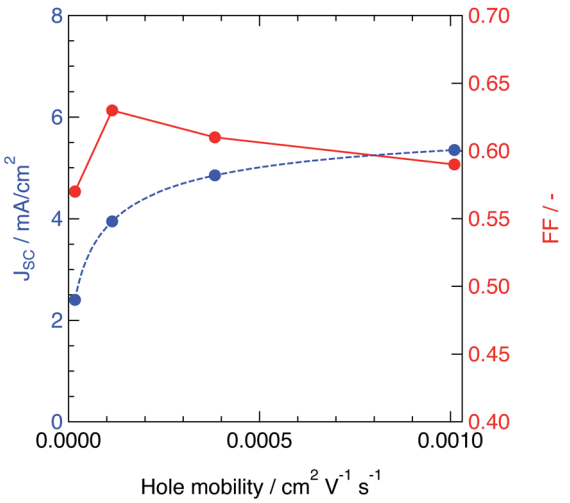


Fig. 9 $J_{SC}$ and FF for OPV cells with BPc films prepared at several temperatures as a function of hole mobility determined from SCLC measurements.

achieving a good linear dependence of $J_{SC}$ and FF on the crystallinity, and thus to good cell performance.

## Conclusions

The thermal conversion behavior of BPc-pre-2 and the film structure of BPc were systematically investigated. The bulky substituents on BPc-pre-2 significantly reduce intermolecular aggregation in the film, which results in smooth and continuous BPc films. The crystallinity of BPc prepared from BPc-pre-2 was strongly dependent on the annealing temperature. The crystallinity increased with annealing temperature, while the surface area of the BPc films prepared from the precursor at temperatures between 150 and 250 °C was almost constant, as determined by AFM. Annealing at 250 °C resulted in a PCE that was 2.5 times higher than that for the cell annealed at 150 °C. The importance of increasing the crystallinity and mobility for improving device performance was experimentally confirmed.

## Experimental section

BPc-pre-1 and BPc-pre-2 were readily dissolved in dichloromethane to give saturated concentrations of 0.15% and 0.7% (w/w), respectively. BPc-pre-1 films were prepared on ITO/PEDOT:PSS substrates by spin-coating with a saturated BPc-pre-1 dichloromethane solution at 1500 rpm. BPc-pre-2 films were formed from a 0.6% dichloromethane solution. Annealing for thermal conversion was conducted at various temperatures under atmospheric conditions. The optical properties of the films were characterized using UV-vis absorption spectrometry (Jasco V-670). The structural change from BPc-pre to BPc was examined using FT-IR spectroscopy (Jasco FT/IR-660 Plus). TG analysis was performed using a VAP-9000 (Ulvac Riko). Film morphologies were observed using AFM (Seiko Instruments SPI 3800N) and TEM (Hitachi H-7100). Electron diffraction patterns of the films were recorded at an acceleration voltage of 100 kV using TEM. The X-ray diffraction (XRD) was carried out with 40 kV, 30 mA CuK$_{\alpha 1}$ radiation by $\theta$–$2\theta$ mode using a Rigaku Superlab.

Hole-only devices were fabricated with PEDOT:PSS and Au electrodes as the anodes and cathodes, respectively, to measure SCLC and determine the hole mobilities. A 60 nm-thick Au electrode was deposited on the prepared ITO (200 nm)/PEDOT:PSS (30 nm)/BPc (50 nm) cell for measurement of the hole mobility. The electron mobility of PCBM was measured with the electron-only device [Al (80 nm)/LiF (0.5 nm)/PCBM (60 nm)/LiF (0.5 nm)/Al (80 nm)]. The electrical characteristics were measured in the dark using Keithley 4200 source/measure units.

The common structure of PHJ cells was as follows: ITO (200 nm)/PEDOT:PSS (30 nm)/BPc (50 nm)/PCBM (30 nm)/LiF (0.5 nm)/Al (60 nm). The BPc layer was fabricated by spin-coating an ITO/PEDOT:PSS substrate with a 0.15% (BPc-pre-1) or 0.6% (BPc-pre-2) dichloromethane solution and subsequent annealing at 150, 170, 200, or 250 °C for different intervals. A 50 nm-thick vacuum-deposited BPc film was formed at a deposition rate of 0.1 nm min$^{-1}$. Each cell was spin-coated with a

 

PCBM layer (30 nm) using a toluene solution. LiF and Al were then vacuum-deposited as the opposite electrode. The *J–V* characteristics of the OPV cells were measured in air under 100 mW $cm^{-2}$ light illumination (AM 1.5) at room temperature and without encapsulation of the devices.

## Acknowledgements

This work was supported by Grants-in-Aid (no. 25706019 to M.M. and no. 22350083 to H.Y.), the Japan Science and Technology Agency (JST) A-STEP program, and the Green Photonics Project of the Nara Institute of Science and Technology (NAIST) sponsored by the Ministry of Education, Culture, Sports, Science and Technology (MEXT) of Japan. The authors thank Yoshiko Nishikawa for conducting electrospray ionization-mass spectrometry (ESI-MS) measurements. We acknowledge the Nippon Synthetic Chem. Ind. (Osaka, Japan) for a gift of ethyl isocyanoacetate, which was used for the preparation of the starting pyrroles.

## Notes and references

1 (*a*) C. J. Brabec, S. Gowrisanker, J. J. M. Halls, D. Laird, S. J. Jia and S. P. Williams, *Adv. Mater.*, 2010, **22**, 3839; (*b*) B. Walker, C. Kim and T. Q. Nguyen, *Chem. Mater.*, 2011, **23**, 470–482; (*c*) Y. Yong, F. Lia and X. Zhan, *Chem. Soc. Rev.*, 2012, **41**, 4245–4272; (*d*) P. Kumar and S. Chand, *Prog. Photovoltaics*, 2012, **20**, 377–415; (*e*) Y. Sun, G. C. Welch, W. L. Leong, C. J. Takacs, G. C. Bazan and A. J. Heeger, *Nat. Mater.*, 2012, **11**, 44–48; (*f*) M. Kaltenbrunner, M. S. White, E. D. Głowacki, T. Sekitani, T. Someya, N. S. Sariciftci and S. Bauer, *Nat. Commun.*, 2011, **3**, 770.

2 M. A. Green, K. Emery, Y. Hishikawa, W. Warta and E. D. Dunlop, *Prog. Photovoltaics*, 2012, **20**, 12–20.

3 (*a*) S. Günes, H. Neugebauer and N. S. Sariciftci, *Chem. Rev.*, 2007, **107**, 1324; (*b*) L. Bian, E. Zhu, J. Tang, W. Tang and F. Zhang, *Prog. Polym. Sci.*, 2012, **37**, 1292–1331; (*c*) A. Mishra and P. Bäuerle, *Angew. Chem., Int. Ed.*, 2012, **51**, 2020–2067.

4 (*a*) I. Osaka, T. Kakara, N. Takemura, T. Koganezawa and K. Takimiya, *J. Am. Chem. Soc.*, 2013, **135**, 8834–8837; (*b*) R. Pandey, A. A. Gunawan, K. A. Mkhoyan and R. J. Holmes, *Adv. Funct. Mater.*, 2012, **22**, 617–624; (*c*) H. Bronstein, Z. Chen, R. S. Ashraf, W. Zhang, J. Du, J. R. Durrant, P. S. Tuladhar, K. Song, S. E. Watkins, Y. Geerts, M. M. Wienk, R. A. J. Janssen, T. Anthopoulos, H. Sirringhaus, M. Heeney and I. McCulloch, *J. Am. Chem. Soc.*, 2011, **133**, 3272–3275; (*d*) C. Schünemann, D. Wynands, L. Wilde, M. P. Hein, S. Pfützner, C. Elschner, K.-J. Eichhorn, K. Leo and M. Riede, *Phys. Rev. B: Condens. Matter Mater. Phys.*, 2012, **85**, 245314; (*e*) R. R. Lunt, J. B. Benziger and S. R. Forrest, *Adv. Mater.*, 2010, **22**, 1233–1236; (*f*) J. D. Zimmerman, X. Xiao, C. K. Renshaw, S. Wang, V. V. Diev, M. E. Thompson and S. R. Forrest, *Nano Lett.*, 2012, **12**, 4366–4371; (*g*) G. Wei, X. Xiao, S. Wang, K. Sun, K. J. Bergemann, M. E. Thompson and S. R. Forrest, *ACS Nano*, 2011, **6**, 972–978.

5 (*a*) Y. Kim, S. A. Choulis, J. Nelson, D. D. C. Bradley, S. Cook and J. R. Durrant, *Appl. Phys. Lett.*, 2005, **86**, 063502; (*b*) G. Li, V. Shrotriya, J. Huang, Y. Yao, T. Moriarty, K. Emery and Y. Yang, *Nat. Mater.*, 2005, **4**, 864; (*c*) Y. Zhao, Z. Xie, Y. Qu, Y. Geng and L. Wang, *Appl. Phys. Lett.*, 2007, **90**, 043504; (*d*) J. Jo, S.-I. Na, S.-S. Kim, T.-W. Lee, Y. Chung, S.-J. Kang, D. Vak and D.-Y. Kim, *Adv. Funct. Mater.*, 2009, **19**, 2398–2406; (*e*) H. Hoppe and N. S. Sariciftci, *J. Mater. Chem.*, 2006, **16**, 45–61; (*f*) M. T. Dang, L. Hirsch, G. Wantz and J. D. Wuest, *Chem. Rev.*, 2013, **113**, 3734–3765.

6 (*a*) S. Ito, T. Murashima, N. Ono and H. Uno, *Chem. Commun.*, 1998, 1661; (*b*) H. Yamada, T. Okujima and N. Ono, *Chem. Commun.*, 2008, 2957.

7 Y. Matsuo, Y. Sato, T. Niinomi, I. Soga, H. Tanaka and E. Nakamura, *J. Am. Chem. Soc.*, 2009, **131**, 16048.

8 (*a*) J. Strating, B. Zwanenburg, A. Wagenaar and A. C. Udding, *Tetrahedron Lett.*, 1969, **10**, 125–128; (*b*) H. Yamada, C. Ohashi, T. Aotake, S. Katsuta, Y. Honsho, H. Kawano, T. Okujima, H. Uno, N. Ono, S. Seki and K. Nakayama, *Chem. Commun.*, 2012, **48**, 11136–11138.

9 (*a*) P. T. Herwig and K. Mullen, *Adv. Mater.*, 1999, **11**, 480; (*b*) A. Afzali, C. D. Dimitrakopoulos and T. L. Breen, *J. Am. Chem. Soc.*, 2002, **124**, 8812; (*c*) H. Yamada, Y. Yamashita, M. Kikuchi, H. Watanabe, T. Okujima, H. Uno, T. Ogawa, K. Ohara and N. Ono, *Chem–Eur. J.*, 2005, **11**, 6212.

10 A. R. Murphy, J. M. J. Frechet, P. Chang, J. Lee and V. Subramanian, *J. Am. Chem. Soc.*, 2004, **126**, 1596.

11 T. L. Chen, J. J.-A. Chen, L. Catane and B. Ma, *Org. Electron.*, 2011, **12**, 1126.

12 (*a*) T. Akiyama, A. Hirao, T. Okujima, H. Yamada, H. Uno and N. Ono, *Heterocycles*, 2007, **74**, 835; (*b*) A. Hirao, T. Akiyama, T. Okujima, H. Yamada, H. Uno, Y. Sakai, S. Aramaki and N. Ono, *Chem. Commun.*, 2008, 4714.

13 (*a*) D. Kuzuhara, J. Mack, H. Yamada, T. Okujima, N. Ono and N. Kobayashi, *Chem.–Eur. J.*, 2009, **15**, 10060; (*b*) D. Kuzuhara, H. Yamada, S. Mori, T. Okujima and H. Uno, *J. Porphyrins Phthalocyanines*, 2011, **15**, 930.

14 (*a*) H. Saeki, O. Kurimoto, M. Misaki, D. Kuzuhara, H. Yamada and Y. Ueda, *Appl. Phys. Express*, 2013, **6**, 035601; (*b*) H. Saeki, M. Misaki, D. Kuzuhara, H. Yamada and Y. Ueda, *Jpn. J. Appl. Phys.*, 2013, **52**, 111601.

15 T. Okujima, Y. Hashimoto, G. Jin, H. Yamada, H. Uno and N. Ono, *Tetrahedron*, 2008, **64**, 2405–2411.

16 V. D. Mihailetchi, L. J. A. Koster, J. C. Hummelen and P. W. M. Blom, *Phys. Rev. Lett.*, 2004, **93**, 216601.

17 (*a*) V. Shrotriya, Y. Yao, G. Li and Y. Yang, *Appl. Phys. Lett.*, 2006, **89**, 063505; (*b*) C. Melzer, E. J. Koop, V. D. Mihailetchi and P. W. M. Blom, *Adv. Funct. Mater.*, 2004, **14**, 865–870; (*c*) V. D. Mihailetchi, H. Xie, C. Melzer, B. de Boer, J. A. Koster and P. W. M. Blom, *Adv. Funct. Mater.*, 2006, **16**, 699–708.

18 (*a*) G. G. Malliaras, J. R. Salem, P. J. Brock and C. Scott, *Phys. Rev. B: Condens. Matter Mater. Phys.*, 1998, **58**, 13411; (*b*) C. Goh, R. J. Kline, M. D. McGehee, E. N. Kadnikova and J. M. J. Frechet, *Appl. Phys. Lett.*, 2005, **86**, 122110; (*c*) Y. Liang, Z. Xu, J. Xia, S.-T. Tsai, Y. Wu, G. Li, C. Ray and L. Yu, *Adv. Mater.*, 2010, **22**, E135–E138.

19 (*a*) P. W. M. Blom, M. J. M. de Jong and M. G. van Munster, *Phys. Rev. B: Condens. Matter Mater. Phys.*, 1997, **55**, R656; (*b*) V. Shrotriya, Y. Yao, G. Li and Y. Yang, *Appl. Phys. Lett.*, 2006, **89**, 063505.

20 (*a*) L. M. Andersson, C. Müller, B. H. Badada, F. Zhang, U. Würfel and O. Inganas, *J. Appl. Phys.*, 2011, **110**, 024509; (*b*) W. Tress, A. Petrich, M. Hummert, M. Hein, K. Leo and M. Riede, *Appl. Phys. Lett.*, 2011, **98**, 063301; (*c*) B. Qi and J. Wang, *Phys. Chem. Chem. Phys.*, 2013, **15**, 8972–8982; (*d*) G. F. A. Dibb, F. C. Jamieson, A. Maurano, J. Nelson and J. R. Durrant, *J. Phys. Chem. Lett.*, 2013, **4**, 803–808.